Long Period Swell Wave Events on the Norwegian Shelf

B. GJEVIK,* H. E. KROGSTAD,** A. LYGRE*** AND O. RYGG*

*Department of Mechanics, University of Oslo, Blindern, Oslo, Norway
**Oceanographic Company of Norway, Trondheim, Norway
***Christian Michelsen Institute, Fantoft, Bergen, Norway

(Manuscript received 7 July 1987, in final form 10 November 1987)

ABSTRACT

Wave records obtained by Waverider and heave/pitch/roll data buoys on the Norwegian continental shelf have been analysed in order to gain information on spectral characteristics (bandwidth, peak frequency, significant wave height and direction) during severe swell events. The main source of long period swell is the northwestern Atlantic, and extreme events are caused by intense extratropical cyclones moving rapidly in a northeasterly direction. The data show swell energy at periods of 20–25 s and with a maximum significant wave height between 4 and 5 m. By using simple wind and wave models it has been possible to identify different regimes for the evolution of the bandwidth of the swell spectrum which also have been confirmed by observations. The model predictions and data analysis lead to a refinement of the classical ridge line analysis in which both the origin time and duration of the storm may be estimated directly from the evolution of the spectrum. In some cases it has also been found that wave refraction and sheltering effects due to Iceland, and the Faeroe, Shetland, and Orkney islands may affect the swell conditions on certain sections of the Norwegian continental shelf.

1. Introduction

The continental shelf along the western and the northern coast of Norway is exposed to long period swell from the North Atlantic through the windows between Iceland–Faeroe Islands–Shetland islands and to a less extent through the window between the Shetland and Orkney islands. The swell is mainly generated by intense extratropical cyclones which frequently originate in the western part of the North Atlantic east of Newfoundland and move rapidly in a northeasterly direction. Wave records from the Norwegian coast during severe swell events caused by distant storms show typical narrow-peaked swell spectra with considerable energy at periods of 20–25 s and a maximum significant wave height up to 4–5 m. Often the swell and locally generated wind waves appear simultaneously and produce broadbanded spectra with considerable energy at periods longer than 20 s. In one case (January 1983) an event with 9 m significant wave height and a spectral peak period T_p = 21 s was recorded at Trænabanken, (Gjevik et al. 1984; Barstow and Lygre 1985). Due to near resonance conditions, the swell can cause large heave motions of semi-submersible drilling rigs and interfere with other offshore operations. For this reason, there is of considerable practical interest to define the most extreme swell conditions on the Norwegian continental shelf and devise forecasting routines. The wave data examined for this study have been obtained by Waverider and heave/pitch/roll data buoys through various data collecting programs initiated by the off-shore oil activity.

Extremely high long waves with period between 20–25 s and significant wave height up to 12.9 m have been observed in the northeast Pacific Ocean and reported by Earle et al. (1984). They also point out that these very long wave periods are not well accounted for by wave formulations that are commonly used in numerical wave prediction models. The meteorological conditions during some of the events which we have examined resemble those studied by Earle et al., however, we have not recorded as extreme wave heights.

It is well established that ocean waves may propagate over large distances and that the time and space origin of the generating storms may be determined by an analysis of the ridges seen on contour plot of the spectral energy density with respect to frequency and time. The method was first devised by Barber and Ursell (1948), improved by Munk et al. (1963) and used in many subsequent studies among others by Snodgrass et al. (1966) and Cartwright et al. (1977).

The ridge line analysis relies on the assumption that the storm can be regarded as a point source, i.e., that the propagation time and distance of the swell are large compared to the duration and the extent of the storm. The ridge line methods may be used successfully even in more complicated situation as noticed for example by Lawson and Long (1983). It is well known that the extent and the duration of the storm limit the frequency band observed at a particular time and location (Neuman and Pierson 1966). The observational data reported here enable a documentation of these effects

Corresponding author address: Dr. Bjorn Gjevik, Dept. of Mechanics, P.O. Box 1053, University of Oslo, Blindern, Oslo 3, Norway.

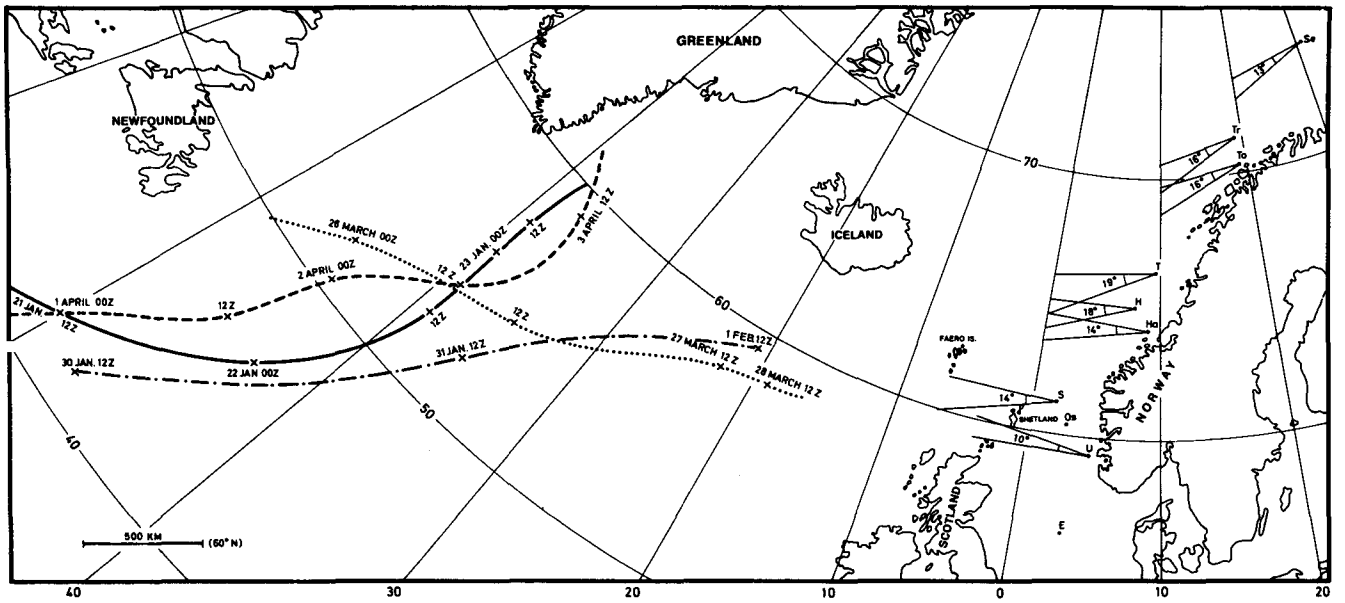

FIG. 1. Map of the North Atlantic and the Norwegian Sea with measurement sites (station symbols in Table 1). Tracks of center of the cyclones; Case I (——), case II (– – –), case III (· · ·) and case IV (–·–).

and a refinement of the ridge line analysis. The spectral peak frequency (f_p) as well as the low and high frequency limits (f_L, f_H) of the swell spectrum are found to be nearly linear functions of time. Predictions based on deep-water wave kinematics and a simplified parameterization of the wave generation mechanism shows that different regimes for the time evolution of f_L, f_H and f_p can be identified and related to the source parameters.

The storms are simulated by a simple circular cyclone model and the time evolutions of f_L, f_H and f_p compare very favorable with the observational data except for some stations where refraction effects may be important. The simulations demonstrate that the ridge line analysis may apply also in cases when the horizontal extent and the duration of the storm are not necessarily small compared to the travel time and distance of the swell. The interpretation of the various slopes and intercepts is, however, more complicated in these cases. Ray tracing indicates that depth refraction due to the shallow banks around the Faeroe and Shetland islands and the eastern part of Iceland affects long periodic swell. In certain situations this may have an important effect on the swell wave height on the Norwegian shelf.

2. Instrumentation and data acquisition

Routine wave measurements in Norwegian waters have taken place since 1969 using waveriders and heave/pitch/roll buoys.

Figure 1 shows the positions of the sensors providing the data used in this study. The corresponding aperture for Atlantic swell is also shown. The water depth at the recording stations range from 70–300 m, cf. Table 1.

The Datawell Waverider Buoy is a moored buoy which records the sea surface elevation by an analogue integration of the signal from a vertical accelerometer. The signal is transmitted by VHF to shore or nearby platforms where it is digitized using a resolution of 0.08 m. The sampling frequency is 2 Hz and a 17 minutes registration is recorded every third hour, cf. Houmb et al. (1974).

The NORWAVE buoys ODAS 490, 492 and 493 are medium-sized wave buoys which combine the ability to measure wave directionality with a variety of meteorological measurements. The buoys consist of discus shaped hulls of diameter 2.5 m (2.75 m for ODAS 492) with a cylindrical instrument section, a subsurface stabilizing steel leg with a ballast weight and a mast for supporting meteorological sensors. The

TABLE 1. Measurement sites.

Station	Position	Sensor	Depth (m)
Sentralbanken (Se)	74°31'N, 31°06'E	ODAS 493	300
Tromsøflaket (Tr)	71°30'N, 19°00'E	Waverider	230
Torsvåg (To)	70°26'N, 19°33'E	Waverider	230
Trænabanken (T)	66°18'N, 09°32'E	ODAS 492	230
Haltenbanken (H)	65°02'N, 07°33'E	ODAS 490	250
Halten (Ha)	64°11'N, 09°09'E	Waverider	190
Statfjord (S)	61°15'N, 01°51'E	Waverider	150
Oseberg (Os)	60°37'N, 02°46'E	ODAS 491	110
Utsira (U)	59°19'N, 04°48'E	Waverider	220
Ekofisk (E)	56°32'N, 03°13'E	Waverider	70

ODAS 491 is a spar buoy basically similar to 490, but without the directional sensor. All buoys are equipped with an Argos satellite transmitter which allows near real time information of buoy performance and meteorological conditions, cf. Audunson et al. (1982).

Data from the buoys undergo a conventional spectral analysis, cf. Eide et al. (1979), Barstow and Krogstad (1984), based on 2048 (or 1024) data points fast Fourier transform with a subsequent averaging corresponding to 16 degrees of freedom (32 dof for the directional data).

Let $S_{\eta\eta}$, S_{xx}, S_{yy}, $S_{\eta x}$, $S_{\eta y}$ and S_{xy} denote the auto and cross-spectra which can be formed from the vertical displacement (η) and the slopes ($\partial\eta/\partial x$, $\partial\eta/\partial y$) time series. The significant wave height, H_{m_0}, is defined

$$H_{m_0} = 4\left(\int_0^\infty S_{\eta\eta}(f)df\right)^{1/2}.$$

The peak period T_p is defined as $1/f_p$ where f_p is the frequency corresponding to the maximum of $S_{\eta\eta}$. The bandwidth is defined by the frequencies f_L and f_H where the spectral level is 0.1 the peak value. The swell significant wave height $(H_{m_0})_{SW}$ is obtained by integrating $S_{\eta\eta}$ over the swell bandwidth.

The directional spectrum is written $F(f, \theta) = S_{\eta\eta}(f)D(\theta, f)$ where D is the directional distribution,

$$D(\theta, f) = \frac{1}{2\pi}[1 + 2\sum_{n=1}^{\infty}(a_n(f)\cos(\theta) + b_n(f)\sin(\theta)].$$

Estimates of a_1, a_2, b_1 and b_2 are obtained as follows:

$$a_1 = \mathrm{Im}(S_{\eta x})/(S_{\eta\eta}(S_{xx} + S_{yy}))^{1/2}$$

$$b_1 = \mathrm{Im}(S_{\eta y})/(S_{\eta\eta})(S_{xx} + S_{yy}))^{1/2}$$

$$a_2 = (S_{xx} - S_{yy})/(S_{xx} + S_{yy})$$

$$b_2 = 2\,\mathrm{Re}(S_{xy})/(S_{xx} + S_{yy}).$$

For details, see Longuet-Higgins et al. (1963) and Long (1980).

In particular, the mean wave direction is defined $\theta_1 = \arctan(b_1/a_1)$ and the circular spreading $\sigma_1 = [2(1 - (a_1^2 + b_1^2)^{1/2}]^{1/2}$. A maximum entropy estimate of D, D_{MEM}, based on a_1, b_1, a_2 and b_2 is defined

$$2\pi D_{MEM}(\theta) = (1 - \phi_1 c_1^* - \phi_2 c_2^*)/|1 - \phi_1 e^{-i\theta} - \phi_2 e^{2i\theta}|^2$$

where

$$\phi_1 = (c_1 - c_2 c_1^*)/(1 - |c_1|^2)$$

$$\phi_2 = c_2 - c_1\phi_1$$

$$c_1 = a_1 + ib_1$$

$$c_2 = a_2 + ib_2$$

and asterisks denote complex conjugate (Lygre and Krogstad 1986).

3. Meteorological conditions and wave observations

Data from a series of swell events on the Norwegian continental shelf was first analysed by Gjevik et al. (1984). We shall summarize the wave observations and the meteorological conditions for four events which are believed to demonstrate important features of long period swell in the region.

Case I: Strong swell was observed all along the Norwegian coast on 24–25 January 1982 and the swell could even be traced in wave records from the sheltered Ekofisk area in the North Sea. Along the western coast wave records were available from Statfjord, Trænabanken and Torsvåg. Since the local wind was light during most of the event, the swell appears as a well defined narrowband peak in the recorded wave spectra.

The swell was generated by an extratropical cyclone originating south of Newfoundland on the 21st. The track followed by the low pressure center is plotted in Fig. 1. The center deepened rapidly with a maximum pressure drop about 20 mb in 3 hours, bringing the pressure at the center down to 955 mb at 0000 UTC on the 22nd. At the same time, a maximum wind speed of 33 m s^{-1} was recorded by a ship at a position (46°N, 41°W). The weather situation is illustrated by the surface weather map in Fig. 2. Between 1200 UTC on the 21st and 1200 UTC on the 22nd the center moved a total distance of about 1600 km leading to a mean propagation speed of about 18 m s^{-1}. This corresponds to the group velocity of 23 s period waves, and suggests that a prolonged fetch may be important for the observed strong energy level for wave components in the 20–25 s period range.

The maximum significant wave height for the swell $(H_{m_0})_{SW}$ = 4.2 m was recorded on Trænabanken at 0300 UTC on the 25th. The peak period was in this case 19.3 s and the bandwidth at 10 dB below the spectral peak (16.6–21.6 s). Longer periods but lower amplitudes were observed earlier and at noon the 24th when the peak period was 23.3 s and $(H_{m_0})_{SW}$ = 2.3 m. The maximum wave heights recorded at Statfjord and Torsvåg were $(H_{m_0})_{SW}$ = 2.2 and 3.0 m with corresponding peak periods at 18.9 and 20.4 s, respectively. Even at Ekofisk a swell significant wave height of 0.7 m and a peak period about 20 s was observed at 1440 UTC on the 24th. The observed evolution of the swell-wave spectrum at Trænabanken, Statfjord, and Torsvåg are visualized by the plots in Fig. 3.

Directional spectra from the heave/pitch/roll buoy at Trænabanken are shown in Fig. 4. The contour plot displays $S_{\eta\eta} \cdot D_{MEM}$. The propagation direction for the swell is from southwest with a mean value of about 260°. The sampling variability of the estimated mean direction is about 12°. This shows that the most likely path for the swell observed at Trænabanken is through the window between Iceland and the Faeroes as indicated by the great circle arcs in Fig. 1.

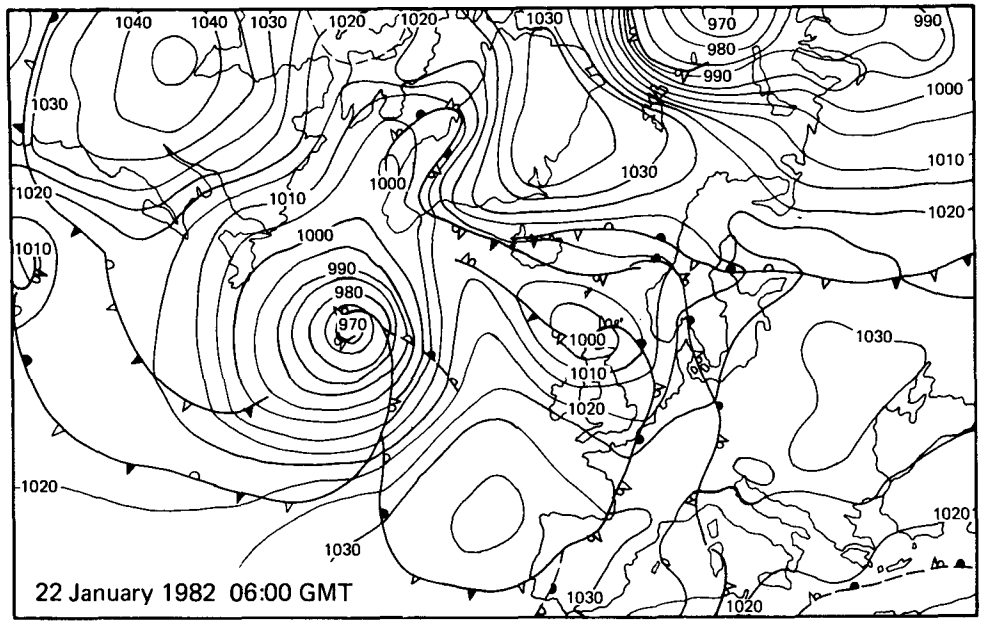

FIG. 2. Surface weather map. Case I.

During a period of about four weeks in March–April 1978 a series of swell events was recorded on the Norwegian coast (Gjevik et al. 1984). The swell was generated by storms in the northwestern Atlantic and since local winds were light during the period, the swell could easily be identified in the measured wave spectra. Two of these events are described in more details below.

Case II: This event occurred on 4–5 April 1978 and was recorded by the Waverider at Halten, Utsira and Tromsøflaket. The swell was caused by an extratropical cyclone on 1–3 April. The weather situation was rather similar to Case I although this cyclone was less intense. The track followed by the cyclone is also shown in Fig. 1. The pressure at the center during the mature stage was about 975 mb with maximum recorded wind speed of 22 m s^{-1}. The rate of pressure drop during the storm development was less than for Case I and the mean propagation speed during the developing and the mature stage was only 13 m s^{-1}. Further details on the meteorological situation can be found in Gjevik et al. (1984).

The swell appeared as a well-defined peak in the spectrum recorded at Halten about 1500 UTC 4 April and the evolution of the swell spectrum could be followed for about 40 hours (Fig. 5). The maximum significant wave height for the swell was about 1.5 m. The swell could be easily identified also in the records from Utsira and Tromsøflaket where the maximum significant wave height was 0.9 and 1 m, respectively. The observational data from Tromsøflaket are presented in Fig. 5.

Case III: The swell generated by a storm in the North Atlantic on 26–28 March 1978 was observed at Halten and Utsira on the 28th and the 29th. This cyclone headed in a more easterly direction than in the previous two cases as indicated by the track in Fig. 1. The pressure at the center was down to 955 mb and the mean propagation speed was about 12 m s^{-1}. The cyclone produced strong southwesterly winds with wind speeds up to 25 m s^{-1} in a region around 50°N, from 45°W to 15°W. Surface weather maps are presented in the report by Gjevik et al. (1984). It is possible to identify the swell in the wave spectrum and read the frequency bandwidth at the 10 db level from the records at Halten and Utsira. The maximum significant wave height of the swell was about 2 m at Halten and 1.8 m at Utsira. The data from the former station are presented in Fig. 6.

Case IV: The storm originated southeast of Newfoundland on 30 January 1985 and the low pressure center followed a track depicted in Fig. 1 with a propagation speed varying from 17 to 13 m s^{-1}. The pressure was down to about 970 mb at 1200 UTC by the 31st and the southwesterly wind field set up by the cyclone (Fig. 7) reached a maximum strength of about 20 m s^{-1}. The swell was recorded by buoys at Haltenbanken and at Sentralbanken in the Barents Sea and also by a waverider at Kråkenes (62°N, 5°E). At Kråkenes local wind sea made it difficult to identify the swell and follow the evolution of the swell spectrum. At Haltenbanken the swell spectrum could be identified only for a relative short time span of about 15 h, while at Sentralbanken it was possible to read the swell spectrum characteristics for about 40 h (Fig. 8). The directional analysis shows that long-period wave energy arriving from other directions than the main source partly con-

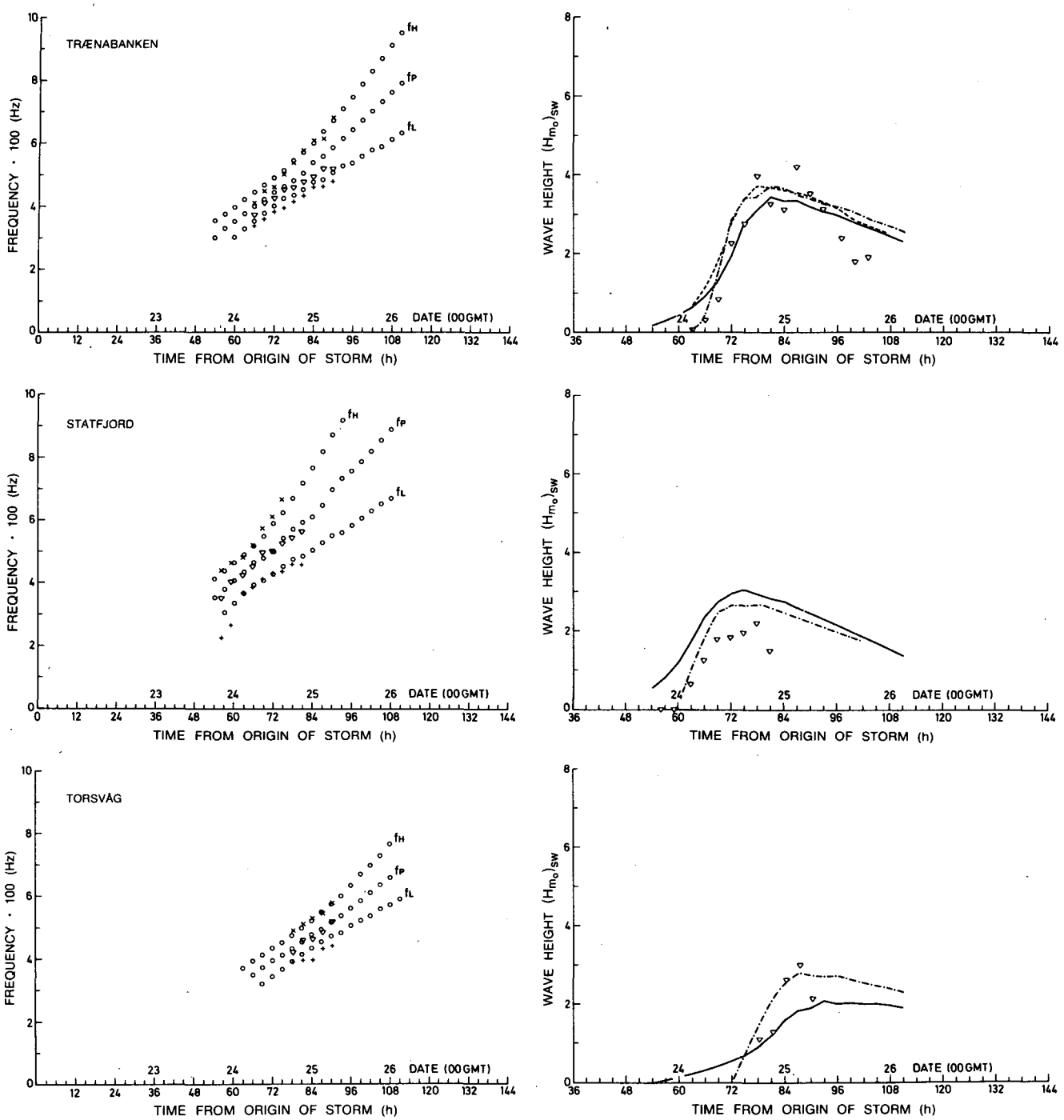

FIG. 3. Case I, January 1982: Swell spectrum observations and model simulations for Trænabanken (upper graphs), Statfjord (middle graphs) and Torsvåg (lower graphs). Left panel: Spectral band-width (f_L, f_H) and peak frequency (f_p). Dotted lines (· · ·) model simulation based on the growth relation (4.7). Observed data (×××), (▽▽▽) and (+++) for f_H, f_p and f_L, respectively. Right panel: Significant wave height for swell: (▽▽▽) observations. Model simulation: with relation (4.7), full drawn lines (——), (–·–) relation (4.6) and (– – –) Darbyshire's relation (see text). All results with great circle paths.

taminates the record. During the first part of the event the noise arrived from east and southeast, but from early on 4 February the noise arrived from north. We have not been able to identify the sources of the noise. It is interesting to note that at the time of observation the edge of the Arctic sea ice was situated about 150

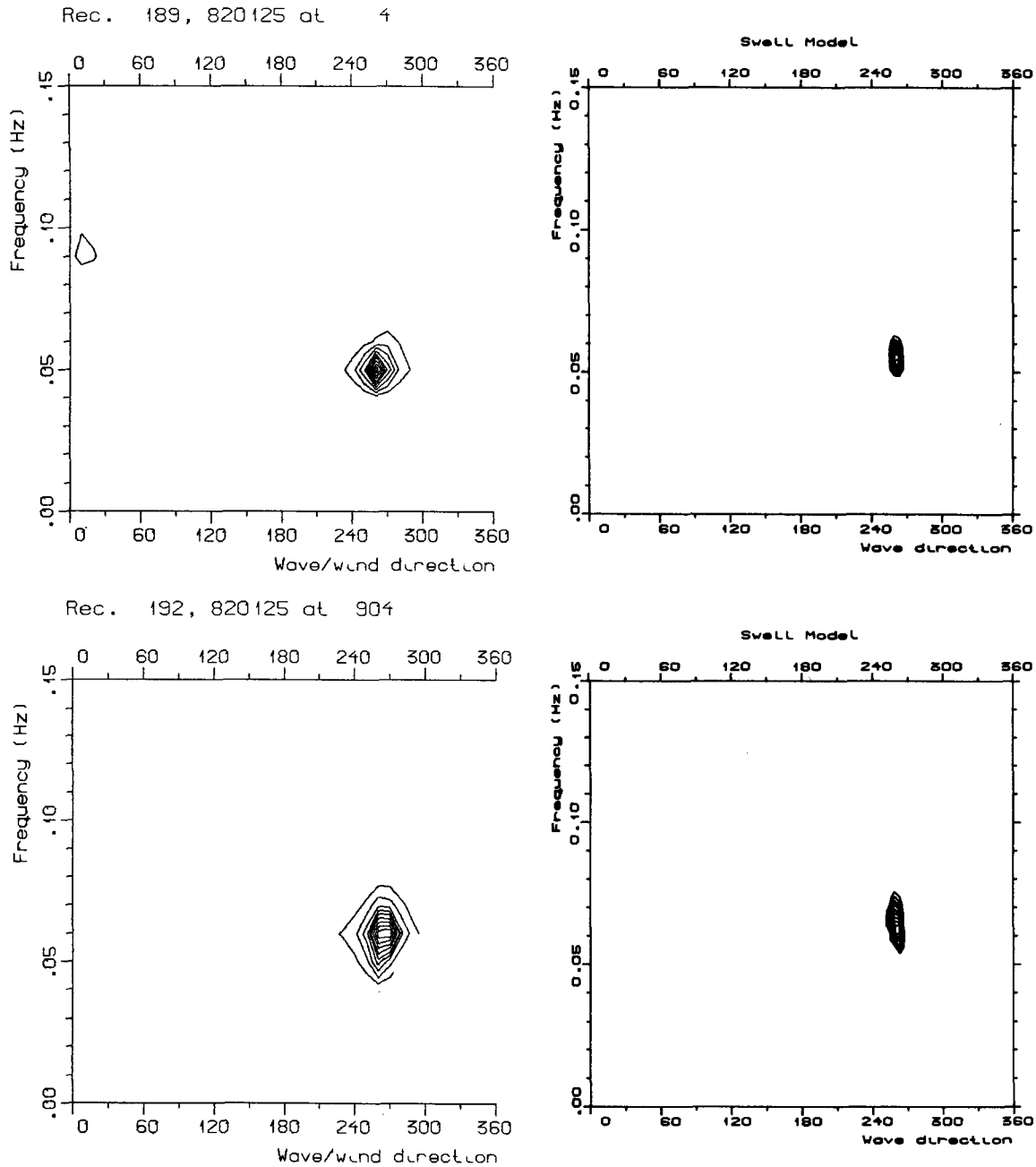

FIG. 4. Observed and predicted directional wave spectrum for Trænabanken, Case I. Records 189 and 192 from 0000 and 0900 UTC 25 January, left panels: Corresponding model predictions, right panels. Contour lines are drawn in steps of 10% of the spectral peak height.

km north of the buoy and that a wide tongue of drifting ice floes stretched southward to Bear Island, located west of the measurement site. The tongue of drifting ice may therefore have affected the incoming swell. The maximum swell significant wave height at Haltenbanken and Sentralbanken was estimated from the records to be 2.8 and 1.9 m, respectively.

4. Model prediction

We shall first review some basic features of swell wave kinematics under idealized conditions. On the first hand, we tacitly assume that refraction effects are negligible and that each wave component moves along great circle paths with the deep water group velocity

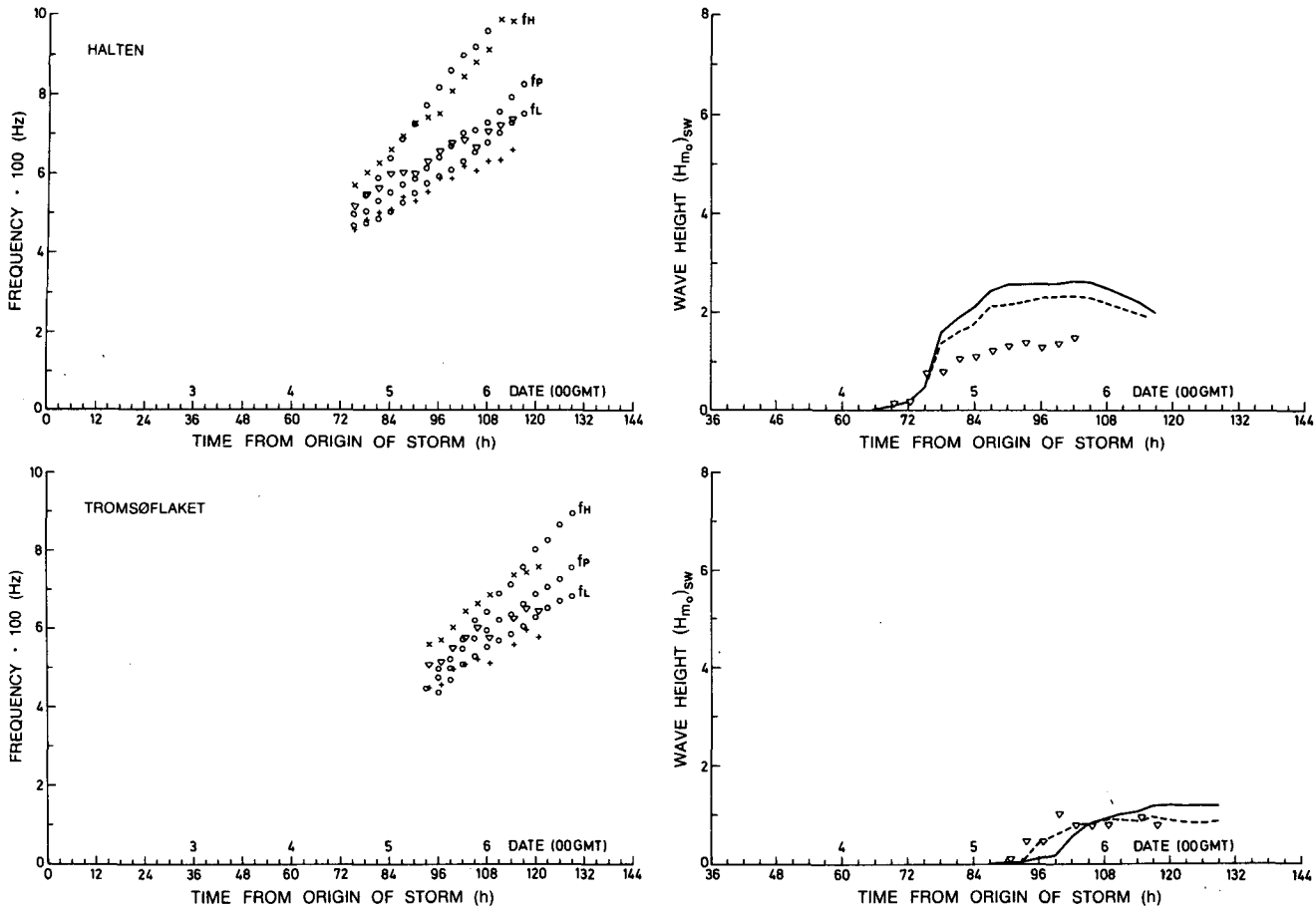

FIG. 5. Case II, April 1978: Swell spectrum observations and model simulations for Halten (upper graphs) and Tromsøflaket (lower graphs). Model simulations with relation (4.7). Predicted wave height with great circles paths (——), with refracted ray paths (– – –). All other symbols as explained in Fig. 3.

$$c_g = \frac{g}{4\pi f}$$

where g is the acceleration of gravity and f is the frequency. Consider waves generated by a moving storm area and observed at the position P with geographical coordinates (ϕ_p, λ_p) which are colatitude and longitude, respectively (see Fig. 9). The wave component arriving at time $t = t_0$ from an azimuth direction θ_p has followed the ray characteristic SP where S is the position of the

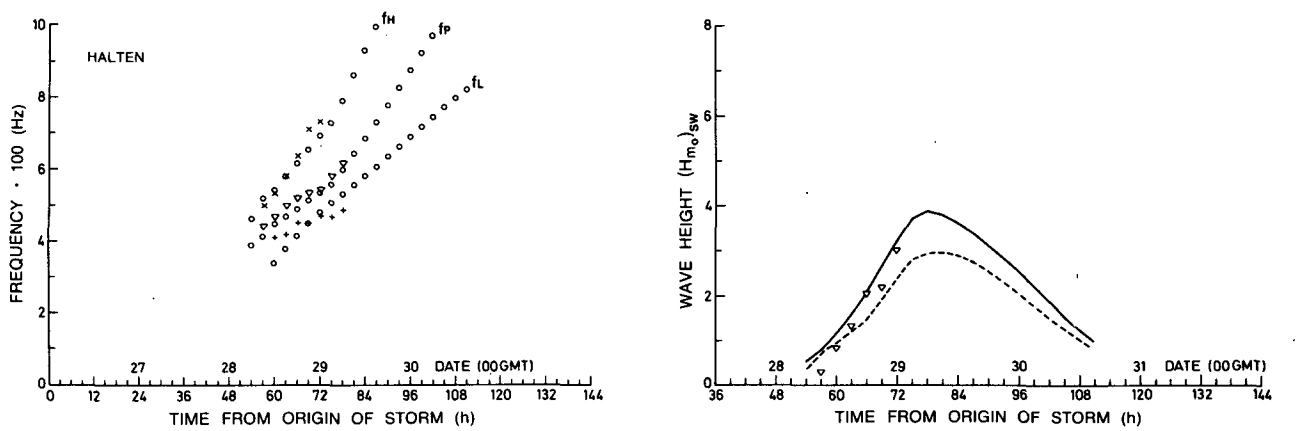

FIG. 6. Case III, March 1978: Swell spectrum observations and model simulations for Halten with the growth relation (4.7). Predicted wave height with great circle paths (——), with refracted ray paths (– – –). All other symbols as explained in Fig. 3.

wave component at time t. If r is the distance SP along the path we obviously have

$$\frac{r}{t_0 - t} = \frac{g}{4\pi f}. \tag{4.1}$$

If the storm area is of finite extent and duration, then only wave components within a certain frequency band $f_L < f < f_H$ will appear at P at a given time. Moreover, the wave components will arrive within a viewing sector defined by an azimuth angle θ where $-\Delta\theta_1 < \theta - \theta_p < \Delta\theta_2$ and the angles $\Delta\theta_1$ and $\Delta\theta_2$ are determined by the geometry of the wind field (cf. Neumann and Pierson 1966; Gjevik et al. 1984). For wind fields that are far away from the observation point P, it is possible to find simple analytical expressions for f_L, f_H, θ_1 and θ_2. If the center of the wind field at $t = 0$ is a distance r_0 from P and is moving towards P along the great circle with constant velocity U and the wind duration is D we have approximately

$$\Delta\theta_1 = \Delta\theta_2 = \frac{B/2}{r_0 - UD - \frac{A}{2}}.$$

Here A and B are the typical length and width of the wind field, respectively, which for simplicity is assumed to be symmetric about an axis in the direction of motion. A straight forward derivation yields for the enclosing frequencies

I) $t_0 < D$: $f_L = 0$, $f_H = \dfrac{g}{4\pi}\dfrac{t_0}{r_0 - \frac{A}{2}}$

II) $D < t_0 < \dfrac{r_0 - \frac{A}{2}}{U}$:

$$f_L = \frac{g}{4\pi}\frac{t_0 - D}{r_0 - UD + \frac{A}{2}}, \quad f_H = \frac{g}{4\pi}\frac{t_0}{r_0 - \frac{A}{2}}$$

III) $\dfrac{r_0 - \frac{A}{2}}{U} < t_0 < \dfrac{r_0 + \frac{A}{2}}{U}$:

$$f_L = \frac{g}{4\pi}\frac{t_0 - D}{r_0 - UD + \frac{A}{2}}, \quad f_H = \frac{g}{4\pi}\frac{t_0 - D}{r_0 - UD - \frac{A}{2}}$$

IV) $\dfrac{r_0 + \frac{A}{2}}{U} < t_0$:

$$f_L = \frac{g}{4\pi}\frac{t_0}{r_0 + \frac{A}{2}}, \quad f_H = \frac{g}{4\pi}\frac{t_0 - D}{r_0 - UD - \frac{A}{2}}. \tag{4.2}$$

These formulas only apply if A, B and UD are small compared with r_0. The more general case is treated by Gjevik et al. (1984). In all four regimes, f_L and f_H are linear functions of t_0, but the slopes and the intercepts with the time axis are different as indicated in Fig. 10. For region III the bandwidth $\Delta f = f_H - f_L$ necessarily

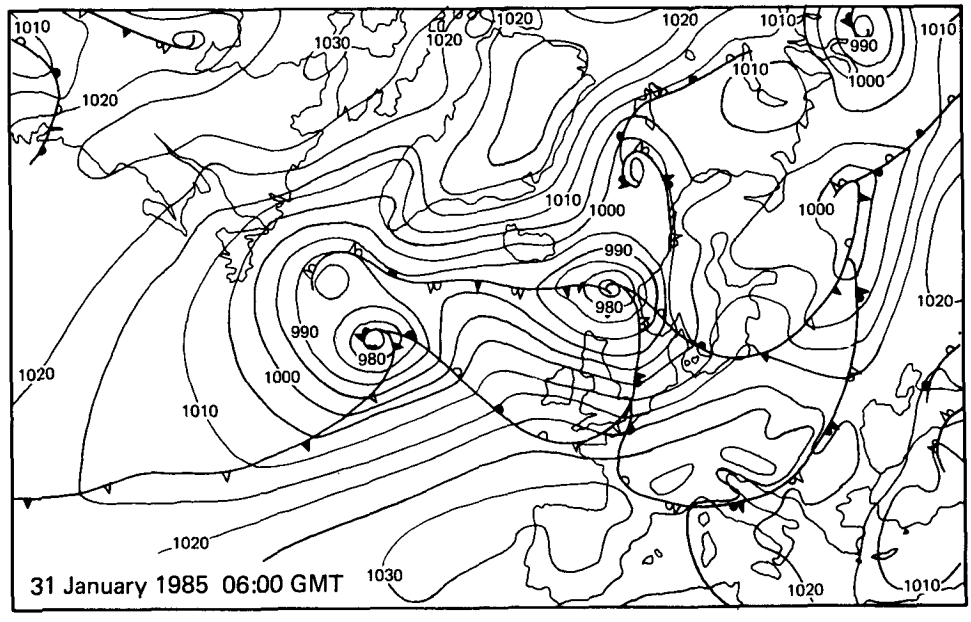

FIG. 7. Surface weather map. Case IV.

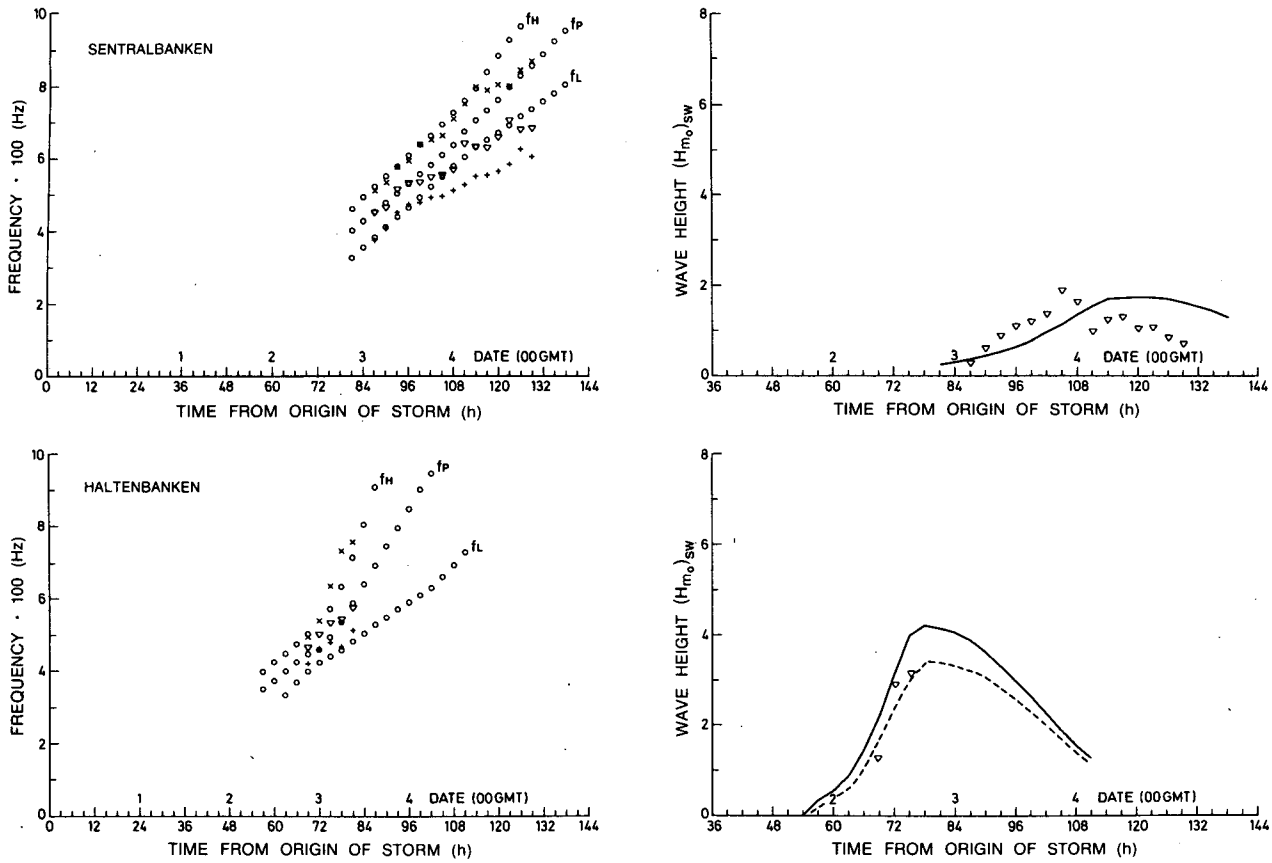

FIG. 8. Case IV, February 1978: Swell spectrum observations and model simulations for Haltenbanken (upper graphs) and Sentralbanken (lower graphs) with growth relation (4.7). Predicted wave height with great circle paths (——), with refracted ray paths (– – –). All other symbols as explained in Fig. 3.

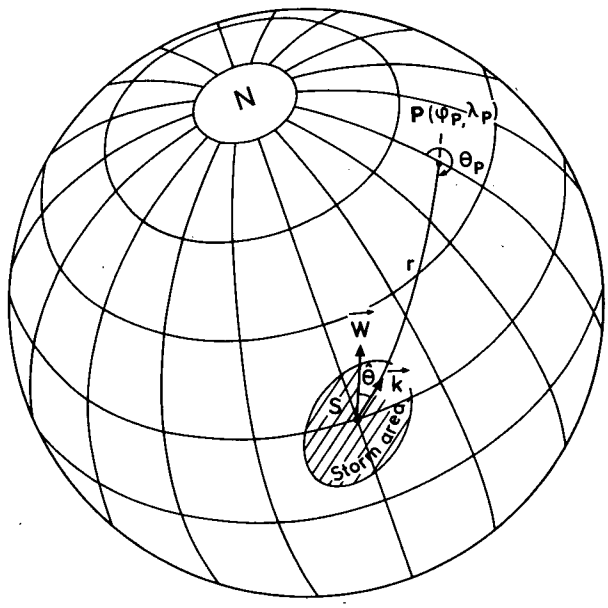

FIG. 9. Definition sketch. Observation point (P) and ray trajectory (PS) towards storm area.

increases with time, whereas for region II Δf may even decrease with time. Furthermore, it is important to note that f_L intercepts the time axis at $t = 0$ and f_H the time axis at $t = D$ for region IV. For region II the opposite is true.

We denote the slopes of f_L and f_H in a f–t_0 diagram by α_L and α_H respectively, and in region II, III and IV we have to the leading order

$$r_0 = \frac{g}{8\pi}\left(\frac{1}{\alpha_L} + \frac{1}{\alpha_H}\right).$$

Similarly, for region IV,

$$A + UD = \frac{g}{4\pi}\left(\frac{1}{\alpha_L} - \frac{1}{\alpha_H}\right)$$

and for region II,

$$A - UD = \frac{g}{4\pi}\left(\frac{1}{\alpha_L} - \frac{1}{\alpha_H}\right).$$

In cases where we are able to identify the limits of region III, these will give A/U directly. In principle, it is therefore possible to obtain all source parameters from an analysis of f_L and f_H versus time.

For given values of f and θ_p the great circle path SP can be determined and the geographical coordinates (ϕ_s, λ_s) for the position of the wave component can easily be traced through the storm area. Hence ϕ_s and λ_s are known functions of time and the rate of change in time of the two-dimensional wave spectrum for a particular wave component can be written

$$\frac{dF}{dt} = Q. \tag{4.3}$$

The source function Q may represent energy input by wind, wave dissipation and energy transfer by nonlinear wave interaction (see Hasselmann et al. 1973). By assuming that the source function Q is a linear function of F it follows by dimensional considerations that

$$Q = g^2 f^{-4} a^*(\pi_1, \pi_2, \pi_3) + f b^*(\pi_1, \pi_2, \pi_3) F \tag{4.4}$$

where a^* and b^* are functions of the nondimensional parameters

$$\pi_1 = \frac{Wf}{g}, \quad \pi_2 = \frac{\rho_a}{\rho_s}, \quad \pi_3 = \hat{\theta}.$$

Here W denotes the wind speed at a fixed reference height, ρ_a and ρ_s the density of air and sea water and $\hat{\theta}$ is the angle between the wind vector $\vec{W}$ and the wavenumber vector $\vec{k}$ (see Fig. 9).

The growth is limited by a saturation condition which is written

$$F(f, \hat{\theta}) \leq F_s(f, \hat{\theta}) \tag{4.5}$$

where

$$F_s(f, \hat{\theta}) = \frac{\alpha}{(2\pi)^4} g^2 f^{-5} \frac{2}{\pi} \cos^2\hat{\theta} \quad -\frac{\pi}{2} < \hat{\theta} < \frac{\pi}{2}$$

and α denotes the Phillip's constant for which we have applied the value $\alpha = 0.0081$.

Different representations of the functions a^* and b^* have been considered in the literature. In our notation the exponential growth relation devised by Snyder et al. (1981) on basis of extensive measurements reads

$$b^* = b_0\left(\frac{W}{c}\cos\hat{\theta} - 1\right), \quad W\cos\hat{\theta} > c \tag{4.6a}$$

$$b^* = 0, \quad W\cos\hat{\theta} < c \tag{4.6b}$$

where the phase velocity which in deep water is $c = 2c_g$ and

$$b_0 = 0.5\pi \frac{\rho_a}{\rho_c} = 2.04 \times 10^{-3}.$$

For a^* which defines the initial linear growth of wave spectrum we have applied

$$a^* = \frac{\alpha}{(2\pi)^4} b^* \cos\hat{\theta}.$$

As an interesting alternative we have also used a modified version of the empirical growth relation proposed by Darbyshire (1983). The functions a^* and b^* are assumed to be powers of the parameter π_1 and in order to limit growth at low frequencies we use

$$a^* = a_0\left(\frac{Wf}{g}\right)^6 \cos\hat{\theta} \tag{4.7a}$$

$$b^* = b_0\left(\frac{Wf}{g}\right) \cos\hat{\theta}. \tag{4.7b}$$

The dimensionless constants a_0 and b_0 are evaluated from the constants determined by Darbyshire on basis of analysis of wave data from Atlantic storms. By matching at wind speed $W = 20$ m s^{-1} we obtained

$$a_0 = 3.23 \times 10^{-7}, \quad b_0 = 8.42 \times 10^{-3}.$$

We note that with (4.7) the wave growth is not limited to frequencies satisfying the condition $W\cos\hat{\theta} > c$. Transfer of energy to low frequencies by nonlinear interaction may therefore be accounted for by this empirical model. For later references we shall also give the expression for the source term (4.3) corresponding to the relation proposed by Darbyshire (1983)

$$Q = (\tilde{\alpha} + F)\tilde{\beta} f^2 W^2 \cos\hat{\theta}$$

with the following values for the constants $\alpha = 0.13$ m^2 s rad^{-1} and $\beta = 4.29 \times 10^{-5}$ s^3 m^{-2}.

It should be stressed that the relations (4.7) as well as the relation proposed by Darbyshire are formulated on purely empirical basis and are not intended to lead to a deeper understanding of the physics of wave growth. These types of relations do however have efficient computational aspects and with proper tuning the relations provide a fairly accurate description of wave growth. The prediction power of the Darbyshire relation has also recently been explored by Elliot (1987).

For simplicity we shall generate wind fields corresponding to extratropical cyclones by a circular cyclone model. The moving pressure field is described by

$$p = \Delta p_0 \exp\{-[(x - x_c)^2 + (y - y_c)^2]/R^2\} \tag{4.8}$$

where the pressure perturbation Δp_0 and the coordinates of the center (x_c, y_c), which are functions of time, refer to Cartesian axis in a stereographic map projection (Fig. 1). The R is a constant defining the horizontal extension of the cyclone. Variation in strength and propagation speed is most easily modeled by a sequence of time intervals each with different piecewise constant values for Δp_0 and the propagation speed U. The time intervals are most conveniently chosen to correspond to main synoptic observation hours.

The wind velocity components u_g and v_g along the

x and y directions are taken to be a fraction of the geostrophic wind components:

$$u_g = -\frac{\sigma}{f\rho_a}\frac{\partial p}{\partial y}$$

$$v_g = \frac{\sigma}{f\rho_a}\frac{\partial p}{\partial x} \tag{4.9}$$

where ρ_a is the density of the air, σ is a positive real number equal or less than unity and f is the Coriolis parameter. Asymmetric wind fields may be simulated by choosing σ as function of x and y. The deflection of the wind velocity vector toward the center due to frictional effect can also easily be accounted for. For very strong cyclones, as for example the extreme deep depression in the North Atlantic on 15 December 1986 (Burt 1987), the gradient wind formula may apply instead of (4.9).

The time evolution of the spectral characteristics at a specified observation point is most conveniently obtained by numerical integration of (4.3) subject to the condition (4.5) and with either set of the growth function (4.6) or (4.7). Details are given by Gjevik and Rygg (1987). The specified input parameters; duration (D), strength (Δp_0) and track coordinates [$x_c(t)$, $y_c(t)$] are determined from weather maps.

Depth refraction of the waves has been modelled by a numerical integration of the ray equations (LeBond and Mysak 1978). On a spherical globe these equations read

$$\frac{d\phi}{dt} = \frac{c_g \sin\alpha}{R}$$

$$\frac{d\lambda}{dt} = \frac{c_g \cos\alpha}{R \sin\phi}$$

$$\frac{d\alpha}{dt} = -\frac{\cos\alpha}{Rk}\frac{\partial\omega}{\partial\phi} + \frac{\sin\alpha}{Rk\sin\phi}\frac{\partial\omega}{\partial\lambda} + \frac{c_g \cos\phi\cos\alpha}{R\sin\phi}$$

where (ϕ, λ) is the geographical coordinates (colatitude, longitude) of the wave group and the direction angle $\alpha + 90°$ is the azimuth of the propagation direction; k is the wavenumber, R is the radius of the globe and $\omega = 2\pi f$ is the angular velocity. The dispersion relation for gravity waves in shallow water reads

$$\omega = \sqrt{gk\tanh(kh)}$$

and the water depth h is a function of ϕ and λ. The gradients $\partial\omega/\partial\phi$, $\partial\omega/\partial\lambda$ are evaluated from the dispersion relation by differentiating with respect to h while k is kept constant. Further details on the method of integration are given by Gjevik and Rygg (1987).

5. Comparison with observations

The comparison between observed and simulated swell data have been focused on the following spectral characteristics: the time evolution of the bandwidth (f_L and f_H) based on the 10% peak power criterion, the spectral peak frequency (f_p) and the significant wave height [$(H_{m_0})_{SW}$]. The results are shown in Figs. 3, 5, 6 and 8. In two of the cases reported here (Case I and IV) it has also been possible to make direct comparisons between the observed and the simulated directional spectra.

Model simulations have been performed with different wave growth relations and results obtained by the relation recommended by Snyder et al. (1981), and the other two relations formulated above are compared in Fig. 3. For cases II–IV the model predictions displayed in Figs. 5, 6 and 8 are obtained with relation (4.7) which provides a reasonably accurate description of wave growth and transfer of energy to longer wave components.

In the cases studied here, however, wave height predictions with the three different growth relations examined above are found to lead to nearly identical results except for long-period wave components. This is basically a consequence of the saturation condition (4.5) and the exact manner in which saturation is achieved seems to be of less importance provided the energy input occur approximately of a correct rate (cf. Elliot 1987). The relation (4.7) as well as the Darbyshire relation lead, however, to a much more satisfactory prediction of spectral bandwidth for the long-period band since the relation (4.6) does not account for nonlinear transfer of energy to long period wave components. In order to obtain satisfactory results with the relation (4.6), a higher wind speed than the wind speed at 5 m height had to be used.

a. Case I (January 1982)

The storm was stimulated by (4.8) and (4.9) with $\sigma = 1$, $\Delta p_0 = 40$ mb, $R = 600$ km and a duration time $D = 30$ h. The propagation speed was $U = 18$ m s^{-1} along a straight path corresponding closely to the track followed by the cyclone during its most active phase between 1200 UTC 21 January and 0600 UTC 22 January (see Fig. 1). The computed time evolution of f_L and f_H for Trænabanken, (Fig. 4), shows a similar time variation as predicted from simple kinematic principles (Fig. 10) and the model data compares very well with the observations. The observed data seem to fall within the region IV and intercepts with the time axis for lines through the f_L- and f_H-data lead to accurate estimates of the time of origin of the storm and the duration time. The simulated peak frequency and the significant wave height also compare well with the observed data. The simulated directional spectrum shows that the energy is centered within a sector with azimuth angle ranging from 255° to 270° and with the spectral peak at about 260°. This agrees well with observations (Fig. 4). The results for Trænabanken are very little affected by wave refraction.

The simulated time variation of f_L and f_H for Statfjord (Fig. 3) also shows the characteristic evolution

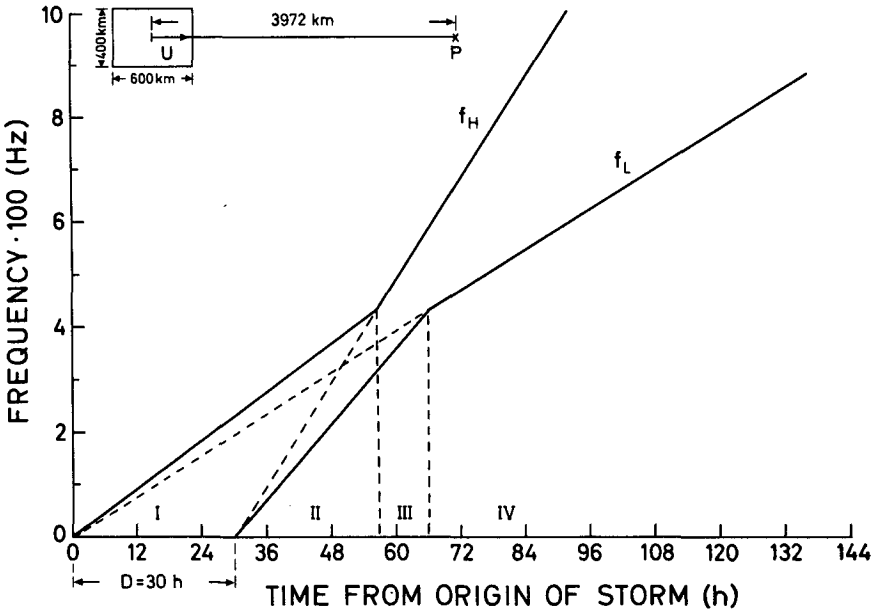

FIG. 10. Swell spectrum generated by a distant storm. Characteristic time evolution of frequency bandwidth at station P. From Eqs. (4.2) with r_0 = 3972 km, U = 18 m s^{-1}, D = 30 h and A = 600 km.

features demonstrated by Fig. 10 and the results compare well with the data. By drawing best fit lines through the f_L and f_H data points, we see that the data covers the transition zone between region II and III. The time of origin can therefore be estimated from the intercept for a line through the f_H points for the first part of the event while the intercept for a line through the later f_H points gives the duration time. The model overpredicts the wave height somewhat (Fig. 3) but since the wind field in this case is located at the edges of the viewing sector from Statfjord the wave height will be sensitive to changes in the spatial distribution of the wind field. In addition, ray tracing shows that the Statfjord area may be strongly effected by wave refraction due to the shallow water in the Faeroe-Shetland region (Fig. 11). Accurate prediction of swell wave height at Statfjord will therefore be difficult in these cases.

For Torsvåg we also find a good correspondence between model prediction and observations for f_L, f_H and f_p (Fig. 4) and the observed data seem to fall in region II. It is therefore interesting to note that the intercepts based on the f_H- and the f_L-line for Torsvåg will give the time of origin of storm and duration respectively, while the opposite was found to be true for Trænabanken. The predicted wave height based on great circle paths is in fair agreement with observations but ray tracing shows that wave height predictions can be significantly affected by wave refraction along the eastern coast of Iceland and in the Faeroe region (Fig. 11). For this reason accurate predictions of swell wave height for the Torsvåg region will be difficult particularly in cases when the wind field moves at the edges of the viewing sector.

b. Case II (April 1978)

The storm lasted from 1200 UTC 1 April to 0000 UTC 4 April with the most active phase between 0000 UTC 2 April and 0000 UTC 3 April. For this period we estimated Δp_0 to be 38 mb, R = 500 km and the mean propagation speed U = 11 m s^{-1}. The computed time evolution of f_L and f_H for Halten (Fig. 5) compares well with observations and the time duration of the active phase of the storm can be estimated from the intercepts with the time axis of the lines through f_L and f_H, respectively. The computed significant wave height based on great circle paths is somewhat higher than observed. Wave refraction leads to a reduction of wave amplitudes but predictions are still higher than observations.

Model predictions of f_L for Tromsøflaket (Fig. 5) agree well with observations but the agreement is less satisfactory for f_H particularly in the early part of the event.

As for Torsvåg, Case I, we find that the predicted wave height is affected significantly by wave refraction and the computed wave height based on refracted ray paths is found to agree well with observations.

c. Case III (March 1978)

The storm in this case headed in a more easterly direction than in the previous cases. It was simulated in its most active phase between 0000 UTC 26 March, and 2100 UTC 27 March, (duration time D = 42 h) with σ = 1, Δp_0 = 35 mb, R = 600 km and U = 12 m s^{-1}. The computed values of f_L, f_p and significant wave height agrees well with observations at Halten (Fig. 6).

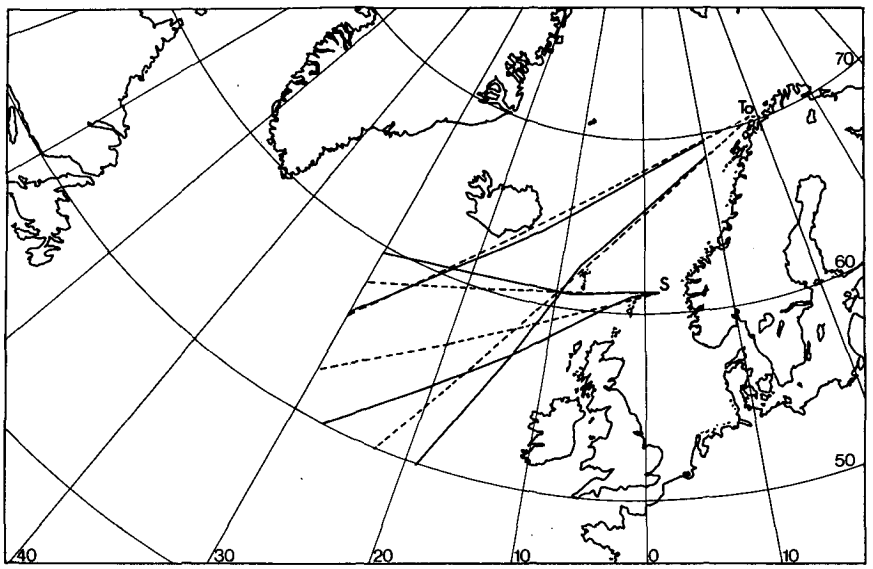

FIG. 11. Ray tracing from Torsvåg (To) and Statfjord (S). Great circle path (- - -) and the corresponding depth refracted rays (full drawn lines) for 20 s period waves.

The intercept with the time axis for the f_p points provides an accurate estimate of the time of origin. Similar analysis based on f_H or f_L does not in this case provide a correct estimate of origin or the duration time probably due to sheltering effects.

d. Case IV (February 1985)

Since the swell generating wind field in this case is located at the edges of the viewing sectors both from Haltenbanken and Sentralbanken, accurate model predictions are obviously difficult. The storm was simulated in its most active phase between 1200 UTC 31 January and 1200 UTC 1 February with $\sigma = 1$, $\Delta p_0 = 30$ mb, $R = 600$ km, and $U = 17$ m s^{-1}. The computed evolution of the swell spectrum is compared with the observations from Haltenbanken and Sentralbanken in Fig. 8. The model prediction of frequency bandwidth at Sentralbanken agrees well with observations for the early part of the event. Later in the event the observed data is shifted towards lower frequencies than predicted by the model. This may be due to damping effect of sea ice (see above) but unfortunately it is not possible to document this suggestion from the present dataset.

Model predictions infer that the swell from the Atlantic storms will arrive at Sentralbanken from an azimuth angle from 250° to 260°. This compares well with the observations which show that the swell from the main source arrived at azimuth angle between 240° and 280°. Also the predicted significant wave height at Sentralbanken agrees reasonably well with the observations. At Haltenbanken the observed time variation of f_L, f_H and f_p agree well with model prediction. The predicted maximum significant wave height for refracted ray paths is 3.3 m and the observed value is 3.1 m.

5. Conclusions

The main source of long period swell waves on the Norwegian continental shelf is the area in the North Atlantic between 45° and 60°N, 20° and 50°W which is known for its rough wave climate, Bales et al. (1982). The extreme events caused by intense extratropical cyclones moving rapidly in a northeasterly direction may lead to narrowly peaked swell spectra with considerable energy at periods above 20 s.

In cases when the swell and the local wind waves are well separated in frequency, the observed swell spectra show a characteristic time evolution in accordance with predictions based on linear wave kinematics. By using simple wind and wave models it has been possible to identify different regimes for the evolution of the spectral bandwidth which also are confirmed by the observations.

The model prediction leads to a refinement of the classical ridge line analysis and it has been shown that both the time of origin and the storm duration can be estimated from the time evolution of limiting frequencies of the swell spectrum. In cases where the observed swell mainly originates during a limited period of the storm's life time, e.g., due to sheltering effects, the duration of this time interval can be estimated.

The agreement between model predictions and observations is in general best for the central region on the continental shelf, that is stations T, H and Ha (symbol definition in Table 1). These stations are often centered in the main propagation direction of the storms and also have a relatively wide viewing sector open toward the main source area (Fig. 1). For stations on the northern and southern part of the shelf the viewing sector toward the main source area is limited by blocking islands; Iceland, Faeroe Island, Shetland

and the Orkneys. The occurrence of Atlantic swell at the stations on the northern and southern part of the shelf is therefore sensitive to the spatial distribution of the wind field and wave refraction effects as indicated clearly by the model predictions. Reliable model prediction will in these cases require a higher resolution wind model and incorporation of wave refraction effects and sheltering effects.

It should be emphasized that the theoretical results presented here are obtained from a simple wind and wave model where the wind is determined by a circular cyclone model and with wave growth according to different empirical growth relations. It is surprising to see how well simple models predict characteristic and important features of the evolution of the swell spectrum. This is, in particular, true for the frequency limits of the spectral peak f_L and f_H (defined above) which in the absence of sheltering objects depend essentially on the geometry and the motion of the wind field and wave kinematics. Predictions of peak frequency f_p and significant wave height $(H_{m_0})_{SW}$ are also in reasonably good agreement with observations. This shows that even a simple heuristic growth relation can be used to accurately predict the basic evolution characteristics of the swell wave spectrum.

Operational predictions are, however, likely to be improved significantly by a refined wind model which also resolves mesoscale variability of the wind field particularly in cases where sheltering effects are important.

Acknowledgments. This manuscript has been prepared under the Analysis of Oceanographic Data (ANODA) Research Programme funded by Conoco Norway, Inc., A/S Norske Shell, Elf Aquitaine Norge A/S, Total Marine Norsk A/S, Statoil, Saga Petroleum A/S, Norsk Hydro A/S and The Royal Norwegian Council for Scientific and Industrial Research. We greatly appreciate the programme Steering Committee's permission to publish this material. We should also like to thank the sponsors of the Ocean Data Aquisition Programme (ODAP).

REFERENCES

Audunson, T., S. F. Barstow and H. E. Krogstad, 1982: Analysis of wave directionality from a heave, pitch and roll buoy operated offshore Norway. *Ocean Sci. Eng.*, 7(8), 291–319.

Bales, S. L., W. E. Cummings and E. N. Comstock, 1982: Potential impact of twenty year hindcast wind and wave climatology on ship design. *J. Mar. Technol.*, **19**, 11–139.

Barber, N. F., and F. Ursell, 1948: The generation and propagation of ocean waves and swell. *Phil. Trans. Roy. Soc. London*, **A240**, 527–560.

Barstow, S. F., and H. E. Krogstad, 1984: General analysis of directional ocean wave data from heave/pitch/roll buoys. *Modelling Ident. Cont.*, **5**, 47–70.

——, and A. Lygre, 1985: Extreme Atlantic depressions during winter 1982–83: Effects seen in Norwegian Waters. *Weather*, **40**(1), 2–10.

Burt, S. D., 1987: A new North Atlantic low pressure record. *Weather*, **42**, (2), 53–56.

Cartwright, D. E., J. S. Driver and Joyce E. Tranter, 1977: Swell waves at Saint Helena related to distant storms. *Quart. J. Roy. Meteor. Soc.*, **103**, 655–683.

Darbyshire, J., 1983: Numerical prediction of wave characteristics. Rep., University College of North Wales. Bangor.

Earle, D. M., K. A. Bush and G. D. Hamilton, 1984: High-height long-period ocean waves generated by a severe storm in the northeast Pacific ocean during February 1983. *J. Phys. Oceanogr.*, **14**, 1286–1299.

Eide, L. I., H. Krogstad, K. Torsethaugen and S. Tryggestad, 1979: *Proc. Analysis of Wave Spectra From the Norwegian Continental Shelf.* POAC, Vol. 1, Trondheim, 547–781.

Elliott, A. J., 1987: Wave prediction by an empirical ray tracing model. *Proc. Conf. Modelling the Offshore Environment.* London, Soc. Underwater Technol.

Gjevik, B., and O. B. Rygg, 1987: The ANODA swell model. Theory and model simulations. Continental Shelf Institute, Norway, Rep. 25/87.

——, A. Lygre and H. E. Krogstad, 1984: Ocean swell on the Norwegian continental shelf. Continental Shelf Institute, Norway Rep. 6201/1/84.

Hasselmann, K., T. P. Barnett, E. Bouws, H. Carlson, D. E. Cartwright, K. Enke, J. A. Ewing, H. Gienapp, D. E. Hasselmann, P. Kruseman, A. Meerburg, P. Müller, D. J. Olbers, K. Richter, W. Sell and H. Walden, 1973: Measurements of wind-wave growth and swell decay during the joint North Sea wave project (JONSWAP). *Dtsch. Hydrogr. Z.*, (Suppl.) A, **8**(12).

Houmb, O. G., B. Pedersen and P. Steinbakke, 1974: The Norwegian Wave Climate Study. *Proc. International Symp. of Ocean Wave Measurements and Analysis*, New Orleans, Amer. Soc. Civil Eng.

Lawson, L. M., and R. B. Long, 1983: Multimodal properties of the surface wave field observed with pitch-roll buoys during GATE. *J. Phys. Oceanogr.*, **13**, 3, 474–486.

LeBond, P. H., and L. A. Mysak, 1978: *Waves in the Ocean.* Elsevier.

Long, R. B., 1980: The statistical evaluation of directional spectrum estimates derived from pitch/roll buoy data. *J. Phys. Oceanogr.*, **10**, 944–952.

Longuet-Higgins, M. S., D. E. Cartwright and N. D. Smith, 1963: Observations of the directional spectrum of sea waves using the motions of a floating buoy. *Ocean Wave Spectra*, Prentice-Hall, 111–136.

Lygre, A., and H. E. Krogstad, 1986: Maximum entropy estimation of the directional distribution in ocean wave spectra. *J. Phys. Oceanogr.*, **16**, 12, 2052–2060.

Munk, W. H., G. R. Miller, F. E. Snodgrass and N. F. Barber, 1963: Directional recording of swell from distant storms. *Phil. Trans. Roy. Soc. London*, **A255**, 505–584.

Neumann, G., and W. J. Pierson, 1966: *Principles of Physical Oceanography*, Prentice-Hall.

Snodgrass, F. E., G. W. Groves, K. F. Hasselmann, G. R. Miller, W. H. Munk and W. H. Powers, 1966: Propagation of ocean swell across the Pacific. *Trans. Roy. Soc., London*, **A259**, 431–797.

Snyder, R. L., F. W. Dobson, J. A. Eliott and R. B. Long, 1981: Array measurements of atmospheric pressure fluctuation above surface gravity waves. *J. Fluid Mech.*, **102**, 1–59.